CHALMERS
UNIVERSITY OF TECHNOLOGY

Design and evaluation of wind-resistant UAV loitering patterns for sea rescue missions

Analysis and evaluation of autonomous fixed-wing flight patterns for maritime search and rescue operations under varying wind conditions

Master's thesis in Mobility Engineering

Arvid Sundberg

DEPARTMENT OF MECHANICS AND MARITIME SCIENCES
CHALMERS UNIVERSITY OF TECHNOLOGY
Gothenburg, Sweden 2026
www.chalmers.se

Master's Thesis in Mobility Engineering

Analysis and evaluation of autonomous fixed-wing flight patterns for maritime search and rescue operations under varying wind conditions

Arvid Sundberg

Department of Mechanics and Maritime Sciences
Division of Fluid Dynamics
Chalmers University of Technology
Gothenburg, Sweden 2026

Analysis and evaluation of autonomous fixed-wing flight patterns for maritime search and rescue operations under varying wind conditions

Examiner: Carlos Xisto, Fluid dynamics Department
Supervisor: Arion Pons, Fluid dynamics Department
Supervisor: Fredrik Falkman, Swedish Sea Rescue Society
Supervisor: Alexander Sandström, Remote.aero

Master's Thesis 2026
Department of Mechanics and Maritime Sciences
Chalmers University of Technology
SE-412 96 Gothenburg
Sweden
Telephone +46 31 772 1000

Cover: Picture of SSRS drone captured by Fredrik Falkman (SSRS).

Typeset in LaTeX
Gothenburg, Sweden 2026

Design and evaluation of wind-resistant UAV loitering patterns for sea rescue missions
Analysis and evaluation of autonomous fixed-wing flight patterns for maritime search and rescue operations under varying wind conditions
ARVID SUNDBERG
Department of Mechanics and Maritime Sciences
Division of Fluid Dynamics
Chalmers University of Technology

Abstract

Fixed-wing Unmanned Aerial Vehicles are increasingly being utilized in maritime Search and Rescue (SAR) operations due to their superior flight endurance and aerodynamic efficiency compared to a multi-rotor system like a quadcopter. However, unlike rotary-wing UAVs, a fixed-wing aircraft cannot effectively hover over a target area without suffering to stall, since the requirement of maintaining sufficient forward airspeed to generate lift. Loitering maneuvers prove effective in weak winds but significantly worse in stronger wind conditions. The steep bank angles required to maintain the flight path do result in partial obstruction of the onboard camera by the drones own airframe. This in practice does reduce the effectiveness of aerial surveillance during critical rescue missions.

The purpose and goal of this thesis was to investigate whether an alternative flight pattern could improve the overall camera visibility while still maintaining the operational advantages that fixed-wing UAVs do provide. The work focused on the development and evaluation of a structured figure-eight based flight pattern which was intended to minimize camera blockage and reduce the spatial footprint of the maneuver during maritime SAR missions.

The research was conducted entirely within the ArduPilot Software-in-the-Loop simulation environment using ArduPlane. Along with custom Python scripts that were created to automatically generate way point missions and process the captured telemetry data extracted from MAVLink logs. The experiments evaluated how the wind speed, wind direction, pattern scale, and maximum allowed roll angle do affect the outcome on flight stability and also camera visibility. The visibility was analyzed using a geometric field-of-view and line-of-sight model combined with an occlusion criterion based on aircraft bank angle.

The study concludes that carefully configured figure-eight flight paths can enable a fixed-wing UAV to achieve similar surveillance behavior to a hovering multi-rotor UAV while also retaining the advantages that comes with the design choice of a fixed-wing. The findings do provide a technical foundation for future development for UAV flight strategies for maritime SAR missions and also demonstrates how flight-path optimization can help to improve aerial observation capabilities under challenging environmental conditions.

Keywords: UAV, fixed-wing, ArduPilot, pseudo-hover, maritime search and rescue, camera coverage, flight-path optimization, line-of-sight analysis, autonomous flight.

Preface

This report presents the outcome of our master's thesis project carried out at the Department of Mechanics and Maritime Sciences at Chalmers University of Technology during the spring of 2026. The work done is connected to SSRS and their development in use of a fixed-wing UAV in maritime search and rescue missions.

Acknowledgements

I would like to express my sincere gratitude towards Arion Pons at Chalmers University of Technology for his valuable supervision, extensive knowledge within the field of UAVs and continuous support throughout this thesis work. I would also like to thank Fredrik Falkman at the Swedish Sea Rescue Society (SSRS) for giving me the opportunity to carry out this thesis and also letting me help possibly improving the SSRS use of UAVs along with providing important guidance, insight and operational knowledge during the project.

Finally, I would like to thank Alexander Sandström at Remote.aero for contributing with valuable discussions, sharing his own work and perspectives on the topic and encouraging the development of the work even further.

Arvid Sundberg, Gothenburg, June 2026

Glossary

Below is the glossary containing words that have been used throughout this thesis listed in alphabetical order:

Actuator	A device responsible for physically moving or controlling a mechanism in response to control signals.
Aerodynamic	Relating to the interaction between air and a moving object.
Airframe	The mechanical structure of an aircraft excluding propulsion and payload systems.
Autopilot	An onboard flight control system capable of automatically controlling the aircraft.
Bank angle	The angle between the aircraft wings and the horizontal plane during a turn.
Circuitry	The interconnected electronic components forming an electrical system.
Dihedral angle	The upward angle between an aircraft wing and the horizontal plane, contributing to roll stability.
Energy consumption rate	The rate at which energy is used during aircraft operation.
FlyNetSim	A UAV network simulation framework integrating flight and network simulation environments.
Geodetic coordinates	A coordinate system based on latitude, longitude, and altitude used to describe positions on Earth.
Holonomic	A motion system where all degrees of freedom can be independently controlled.
Loiter	A flight mode where the aircraft maintains a circular holding pattern around a fixed point.
LUA	A lightweight scripting language commonly used for embedded system customization and automation.
Mesh network	A decentralized network topology where nodes relay data between one another.
Multiplexer/Failsafe unit	An electronic unit used to switch between signal sources or provide backup control functionality.
NS-3	A discrete-event network simulator commonly used for communication system research.
Occlusion	The obstruction of an object or line-of-sight from view.
Soaring	A flight technique where atmospheric lift is used to maintain altitude with minimal propulsion.

Stall	An aerodynamic condition where airflow separates from the wing, resulting in loss of lift.
Telemetric	Relating to the wireless transmission of measurement and system data.
Trajectory	The flight path followed by an aircraft through space over time.

List of Acronyms

Below is the list of acronyms that have been used throughout this thesis listed in alphabetical order:

API	Application Programming Interface
BWB	Blended Wing Body
FOV	Field of View
GCS	Ground Control Station
GPLv3	GNU General Public License version 3
GPS	Global Positioning System
GUI	Graphical User Interface
HDOP	Horizontal Dilution of Precision
HITL	Hardware in the Loop
IDLC	Iterative Development Life Cycle
LOS	Line of Sight
NFRS	National Firefighting Rescue Service
POI	Point of Interest
RC	Radio Controlled
RLD	Roll Limit Degree
RTL	Return To Launch
SAR	Search and Rescue
SITL	Software in the Loop
SSRS	Swedish Sea Rescue Society
ToT	Time on Target
UAV	Unmanned Aerial Vehicle
VTOL	Vertical Take-Off and Landing
WP	Waypoint
WSL	Windows Subsystem for Linux

Nomenclature

Below is the nomenclature of indices, sets, parameters, and variables that have been used throughout this thesis.

Indices

Sets

Parameters

V_{stall}	Stall speed
g	Gravitational acceleration
R	Turn radius
λ_0	Local datum longitude
φ_0	Local datum latitude

Variables

V	Velocity
F_c	Centripetal force
ϕ	Bank angle
V_{ground}	Ground speed
V_{air}	Air speed
x, y, z	Local coordinate system coordinates
λ	Longitude
φ	Latitude
r_{LOS}	Line-of-sight vector
ΔE	Eastward displacement
ΔN	Northward displacement
ΔD	Vertical displacement
α_h	Horizontal angle
α_v	Vertical angle

Contents

List of Figures

List of Tables

1
Introduction

This section is set out to establish the motivation and foundational framework behind this thesis. It outlines the current challenges in operations in maritime Search and Rescue (SAR) and reviews the existing body of knowledge, which serves as the basis for this work.

1.1 Background

The improvements in the technical section related to UAVs and autonomous systems and their usage have increased, as well as been adopted within the field of search and rescue efforts all over the world, but also in other fields that require visuals of areas difficult for humans to access. To capitalize on this, the Swedish Sea Rescue Society (SSRS) has been working toward setting up its own tactical drone system along the coastal waters to offer its search and rescue teams an instant "hawk eye" perspective over the situation. This way, the search and rescue team will be able to locate the victims faster and have knowledge of the situation before arriving at the scene.

Nevertheless, choosing an appropriate design for the drone that will operate in a challenging environment such as the Arteplago. It requires factoring in various considerations between both the aerodynamics and the operational factors. Figure 1.1 shows the current design of the UAV used by SSRS. It is a fixed-wing UAV and the design choice naturally have superior aerodynamic properties and is more energy-efficient than multi-rotor drones, which are more commonly used in SAR and other applications due to their maneuverability properties. However, the great efficiency comes at a cost in maneuverability, as the fixed-wing design achieves its ability to fly by generating lift from its airfoil. By a forward momentum, the air comes across the plane's wings and leads to the generation of a lifting force. To remove the requirement of a landing strip to generate the initial speed, a catapult launching system has been implemented by SSRS to get the UAV flying. In contrast, a multi-rotor drone achieves lift by spinning its blades to create vertical forces, enabling it to carry out vertical take-off and landings (VTOL) and hover over small areas despite having limitations in terms of operational ranges and payloads [9]. Considering that the organization is a coastal one, the extended range and efficient payload-carrying capabilities of the conventional fixed-wing drone make it the better design choice.

Figure 1.1: Image showing the drone used by SSRS

Although the great baseline effectiveness, the implementation of fixed-wing UAV in the ongoing maritime surveillance creates unique issues with regards to tracking. Current practice within the SSRS involves using loitering flights, where the UAV loops around a designated target in circles with specified altitudes and radius. The fixed-wing platform demonstrates great stability and is safe to perform a stable cruise even in winds higher than 15 m/s [9], but minimizing the radius of the circle is difficult in dynamic wind conditions. If the wind speed exceeds the threshold of 4 m/s, the autopilot is forced to perform a steeper banking in order to counteract any drifting and also maintain its circular trajectory. An extreme rolling maneuver is not harmful to the mission itself but to the image capturing because the tilted body creates a blockage for the camera's field of view in its current placement, which is shown in figure 1.2, during certain parts of the loitering mission. In order to circumvent this issue, this thesis sets its focus on exploring the capabilities of the fixed-wing design in relation to various wind vectors and configuration settings of the autopilot when trying to maximize the camera's visibility during a given loitering pattern.

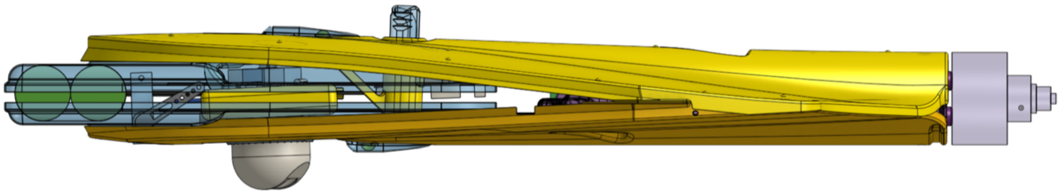

Figure 1.2: Side view of the central body showing the camera placement

1.2 Literature study

The literature study is set to provide an overview of current technologies and approaches utilized in SAR operations, as well as the current trends in UAV research. In addition, explore a bit more the logic of selecting a fixed-wing platform over a multi-rotor one. It will also give insight into the autopilot used by SSRS.

1.2.1 SAR operations in hard-to-reach environments

Unmanned aerial vehicles, also called UAVs, are being integrated into modern search and rescue missions at a growing rate. This is due to their ability to assist with quickly scanning large areas, providing real-time awareness of the situation and at the same time being able to operate in hazardous environments without risking the safety of human personnel [8][9]. By equipping a UAV with different tools like optical, thermal, or even dual-camera payloads, the UAVs provide fundamental support in victim detection, surveillance and also autonomous search paths across different terrains. Early research on the topic focused on the usage of UAVs in SAR and heavily on the conceptual frameworks. Meaning that currently the deployment of UAVs has transitioned from academic theory into a broad usage across global applications for public safety, military, and first responder organizations [13].

Normalizing the usage of UAVs is important to ensure that UAVs are used as a tool in situations where quick action is a key factor and where there may not be enough human labor available to gather large search parties. Systematic review of the operations by the national firefighting rescue service (NFRS), between 2021 and 2023. Poland dispatched firefighters in cases where drone where used to assist the firefighters a total of 780 times[8]. Where a lot of those cases were missing persons searches, in which deployment was mostly carried out in difficult-to-navigate terrain such as forests, water bodies, and rivers. Viewing the large-scale statistics, demonstrated in the paper, the emergency services are already actively relying on very basic UAV usage with different camera mountings depending on application and are continuing their work towards the usage of UAVs specifically designed to speed up the process and increase their capabilities in saving lives. Similar to the goal and usage area for the SSRS and its fixed-wing drone.

Similarly, Jeon et al.[7] developed a real-time drone mapping platform that is capable of generating a geometrically corrected "eagle-eye" imagery and assisting in identifying vessels within seconds. This research led to significant improvements in situational awareness during active marine emergencies. To streamline data processing for ground crews, Messmer et al. [10] proposed the use of an AI-assisted framework enabling onboard object detection to transmit which regions to prioritize and give points of interest. This technology, in synergy, directly minimizes operator workload and accelerates critical decision-making [13]. Within maritime search contexts specifically, Pettersson [14] emphasized how UAVs enhance sea rescue missions by providing early visual feedback, deploying autonomous search algorithms, and also streaming live video to ground crews before they arrive at the scene of the accident. Worth mentioning that Pettersson's work was conducted on an SSRS drone.

In summary, the use of UAVs in the field has been implemented within sectors such as civil defense, firefighting, or even SAR missions around the world. This forms a context-based precedent for maritime organizations like SSRS to implement UAVs into their tool belt. This is where the drone program within the SSRS finds itself. By combining experience in institutional best practices with state-of-the-art sensor technology, the drone usage within the SSRS fits perfectly into the emerging global trends for first responders.

1.2.2 Fixed-wing vs. Multi-rotor

Aerodynamics

When looking at the aerodynamic properties when discussing the fixed-wing vs the rotary UAV design is important to determine their different areas of applicability. When looking at a fixed-wing aircraft, as mentioned earlier, it generates its lifting force by using its wing surfaces and body, hence the need to maintain forward momentum. Whereas the multi-rotor does produce lift directly from the rotors and has the ability to hover without the risk of stall due to its continuous momentum, which is upwards and requires no forward movement. It makes vertical take-offs and conducts precise maneuvers at lower speeds. Consequently, multi-rotor UAVs excel in maneuvering and station-keeping, whereas fixed-wing UAVs typically possess greater aerodynamic efficiency and endurance when it comes to sustained forward flights.

(a) Fixed-wing configuration
(Image source: Uavmodel.com)

(b) Multi-rotor configuration
(Image source: Rawpixle.com)

Figure 1.3: Side-by-side the two different design approches discuessed, (a) a rigid, high efficiency fixed-wing airframe of type Skywalker, and (b) a highly maneuverable multi-rotor quadcopter.

Looking at the work of Panagiotou and Yakinthos (2020)[12], which conducted a literature review of the current UAV designs available, fixed-wing UAVs have better performance at low forward speeds and subsonic flight than the multi-rotor. The authors did highlight several aerodynamic improvements that did increase the UAV's efficiency, including the development of winglets, streamlined fuselages and blended-wing-bodies. Further, Panagiotou and Yakinthos argue that multi-rotor UAVs present a much higher maneuverability and affordability, but they do lack the payload capabilities and endurance compared to the former. This is why, for a thesis that is focused on an ArduPilot-based fixed-wing UAV, these insights prove valuable as they justify the choice of UAV type based on its performance in relation to specific requirements of the application. This also removes the quick solution of switching UAV design.
In an even more recent paper, published by Ye, Wang, Song, Wu and Tang (2021)[22], their paper reveals that the performance of a multi-rotor UAV in forward flight cannot be described by basic hover models. That led to them developing a mathematical nonlinear model that includes such parameters as rotor thrust, pitching and rolling. Their research points to decreased efficiency and control performance as aerodynamic interference effects increase for a multi-rotor UAV.

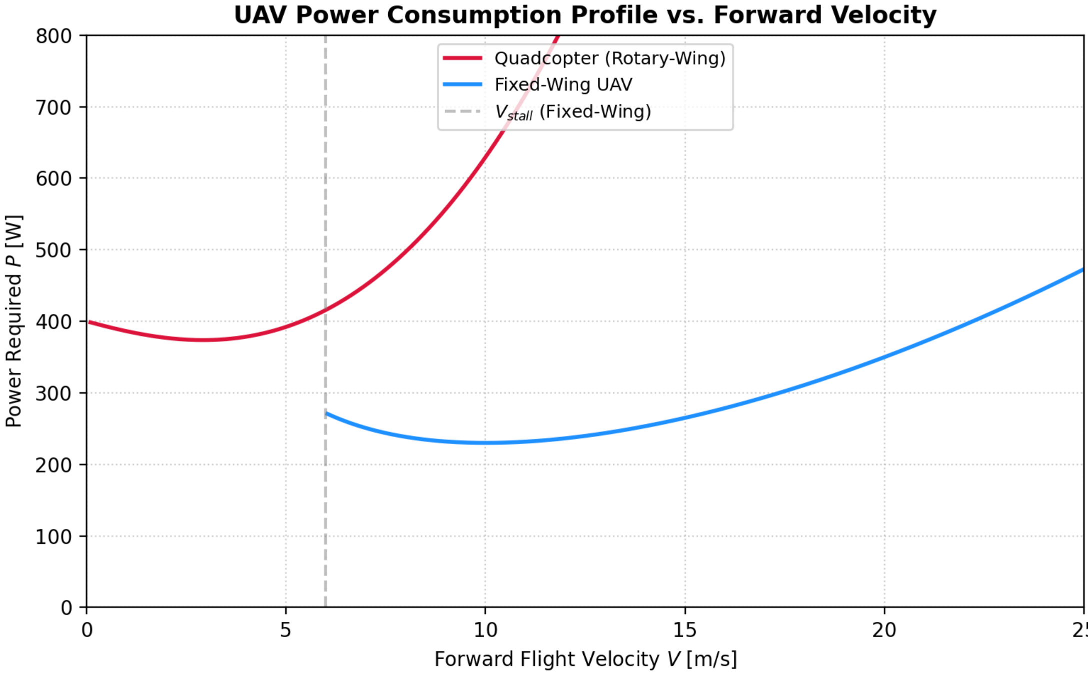

Figure 1.4: Conceptual based power-required profiles versus forward velocity (V), illustrating the low-speed aerodynamic boundary (V_{stall}) for fixed-wing flight and the high-speed parasite drag penalty for multi-rotors.

Energy Consumption

Regarding the utilization of energy for the two UAV designs, the efficiency dilemma in aerial design depends greatly on its mission type. In typical transportation scenarios where the drone has to fly from point A to point B, fixed-wing UAVs will always be more efficient due to the aerodynamic efficiency provided by the lifting surfaces, which reduces the continuous thrust needed from the propulsion system [12]. Therefore, it is common knowledge that increased aerodynamic efficiency results in a longer flight range. In a specific case that involves sharp curved routes, such an efficiency model fails to perform well regarding the flight dynamics. In these specific routes, it's characterized by the need for tight turns and extreme maneuverability of the UAV. The drag losses resulting from banking also result in an increased energy loss profile for the fixed-wing. Analysis of energy consumption for both the fixed-wing and rotary-wing aircraft during such routes reveals that though the two aircraft types have similar energy consumption levels for large orbits, there is a significant efficiency crossover at a small turning radius. The multi-rotor can maintain stability in orbit without a substantial increase in energy consumption, while the fixed-wing aircraft energy consumption increases sharply due to induced drag losses [12].

This energy trade-off presents a critical operational constraint for a fixed-wing UAV executing localized maritime tracking missions. While a multi-rotor configuration offers clear energy and stability advantages during continuous, tight loitering and static hovering maneuvers. It cannot match the high forward transit speeds and aerodynamic efficiency required to span large coastal search areas rapidly. For an operational entity such as the SSRS, the baseline range advantages of a traditional fixed-wing configuration remain highly necessary, shifting the engineering challenge toward mitigating the aerodynamic and energy penalties experienced during high-bank wind-compensation turns.

1.2.3 Hover a fixed-wing during stall-free operation

The compromise between low energy consumption and camera visibility is a vital consideration for operational control of the fixed-wing UAV used by SSRS, through the use of the ArduPlane autopilot for performing more localized maritime tracking tasks and loitering movements.

Figure 1.5: Image of a VTOL UAV
(Image source: universe.roboflow.com/)

One engineering method to overcome this problem with speed is reviewing the design choice of a fixed-wing to the VTOL design, either through tilt-rotors or lift/cruise systems. This design choice would permit the aircraft to be stationary in its hovering mode by switching the control authority of the airplane between the various autopilot routines. By looking at the catalog of ArduPilot firmware, it would mainly involve the switch of architecture from the ArduPlane to the ArduCopter inner loop control algorithm, which is designed for multi-rotor aircrafts [15]. Unfortunately, the VTOL designs will lead to a higher level of mechanical complexity, extra weights from duplicate actuators, and increased energy expenditure in the hovering phase. See figure 1.5 for a VTOL design that could be used. Since it contains the mannerisms of a fixed-wing and a multi-rotor, but due to the design limitations of the current configured fixed-wing drone, this is not a viable solution. If the geometry could be changed, another way to achieve a lower stall speed could be to make a reduction in the total wing loading by utilizing large wings, which have a smaller structural mass. Although this would be effective at low speeds and in stable weather conditions, such a design change will lead to major faults during practical operations. Designs in general that use a lower wing load will experience problems when it comes to aeroelastic instabilities, which result in irregular and destructive vibrations, also known as wing flutter [21, 4]. But again, using a larger wingspan and lower mass, the flutter and irregularities can be limited by a shift in the structural load, but this will cause weakness in the full structure [21, 1]. In the end, design choices that involve changing wing size and shape can be good in theory, but these designs can never survive in harsh weather conditions and do not perform very well in gusty winds.

Given the nature of the SSRS, modifying the physical scale of the airframe design and implementing overly large wing designs is completely off the table. Due to the limitation of using the small airframe design already present, the SSRS requires a stiff and speedy transit, which the fixed-wing UAV can provide. It is able to maneuver through highly turbulent coastal wind gusts of more than 15 m/s. Consequently, the main problem area that has to be solved as part of this research is neither about modifying the physical size of the wings nor about incorporating mechanical VTOL components into the system. The focus will be instead on the optimization of the flight mechanics and the inner-loop control of the small existing fixed-wing UAVs to achieve better visibility.

1.2.4 Soaring flight

Soaring can be defined as the mode of flight that enables an aircraft to gain height through harvesting power from the air itself rather than solely depending on its own rotor. It is a hot topic in order to cut down the power usage of the UAVs with the fixed-wing design, and there are basically two types of soaring. Static soaring, where aerodynamic lift is obtained from localized rising air. Dynamic soaring refers to kinetic energy that is extracted by continually crossing through varying horizontal wind velocities within atmospheric wind shear layers. The dynamic soaring is what birds do to generate lift and speed without the use of too much energy. Soaring maneuvers have been an important part of the practical foundation of crewed glider/sailplanes flights. They are a solid example of the successful implementation of flights at long distances using atmospheric energy without relying on constant energy supplied from engines. The significance of energy conservation is well documented in the classical study of Barringer (1938) [3]. In more recent years, the idea has made its way from manned air travel and biological research to highly technical autonomous aerospace engineering projects. The autonomous soaring project by NASA is one example whereby unmanned aircraft were successfully capable of recognizing and exploiting local thermal zones[11]. The logic behind dynamic soaring and the flight patterns is that they include a loop that is made up of four different stages. First up is a climb towards the wind, then a turn at high altitude, followed by a descent in the direction of the wind, and finally a turn at low altitude. Through such a sequence of maneuvers in a wind gradient (u_z), a sailplane or UAV can save energy by using wind shear energy [19].

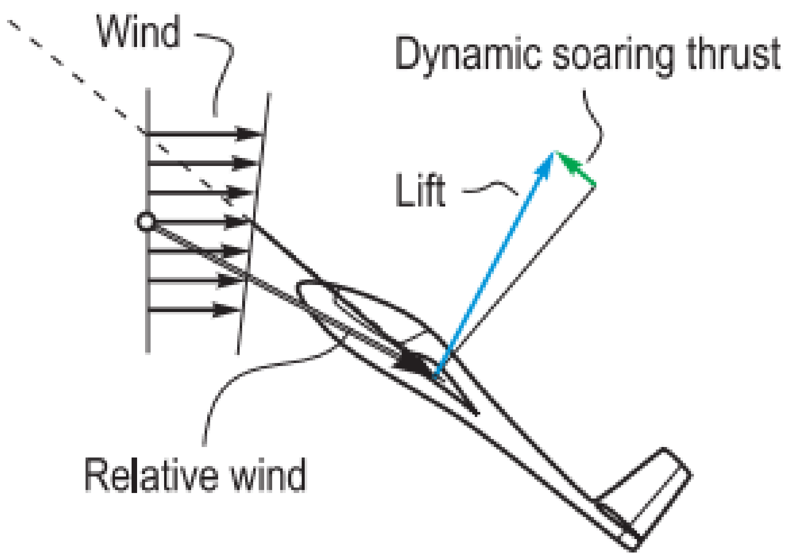

Figure 1.6: Schematic of a dynamic soaring flight trajectory within an atmospheric wind shear profile, highlighting the energy-harvesting phases, adapted from Sukumar and Selig [19].

Boslough (2017) [6] explored autonomous dynamic soaring for UAVs by replicating the precise flight dynamics of an albatross. Validating that lightweight microelectronics can make real-time adjustments within wind shear boundaries highly feasible. In general, while the field of autonomous soaring has matured into a vital domain of aerospace efficiency, its core objective centers on maximum energy preservation. Because the primary objective of this thesis focuses on maximizing camera visibility and ensuring path stability during tight maritime tracking maneuvers, the energy-saving parameters offered by atmospheric soaring fall outside the immediate scope of this operational study[17]. To take full advantage of soaring, it's required to use a larger pattern to be able to obtain/save more energy during flight

1.2.5 ArduPilot as an open-source UAV Ecosystem

ArduPilot is one of the most used open-source flight controllers used for UAVs, especially in cases that require high flexibility and adaptability. ArduPilot also has a huge network of people who help develop and correct issues found within the software. There are two major types of use cases for ArduPilot, first up is employing it as an onboard flight controller, for example a fixed-wing UAV, or secondly, it can be used as a SITL platform for simulations and experimenting with mesh networks of drones and that is how ArduPilot is used for this paper. The article published by Bin and Justice in 2009[5] named "*The design of an unmanned aerial vehicle based on the ArduPilot*", shows an early application of ArduPilot. In which they speak about the design, implementation and testing of an unmanned aerial vehicle which was built on the ArduPilot platform. The controller used was based on ArduPilot and was constructed with a custom PCB with an embedded processor that allows the user to switch between radio control and autopilot control. This was done through the use of a multiplexer/failsafe unit integrated in the build. The navigation capabilities are implemented through a waypoint system and altitude control using actuators to control the rudder and throttle with the inclusion of a GPS module, stability and telemetric units. In the two researchers' work, they did highlight the complete programmability of the system and its capability of navigating several GPS waypoints and triggering cameras or any other sensors, which makes it a good base to build UAVs on. Bin and Justice are highlighting the fact that ArduPilot supports not only navigation but also Return-To-Launch (RTL) functionality, which are both features that continue to be relevant to modern autonomous UAV systems and connect directly to this paper's research topic. This is particularly important to the topic of the current study since it highlights how ArduPilot architecture already allowed for mission logic in its early form. As noted in the article, the drawback at the time was that the waypoints were manually entered before flight and could not be changed during flight. which is something that have evolved and been introduced in to the ArduPilot software which allows you to fly the drone in guided mode meaning, placing WPs in real time.

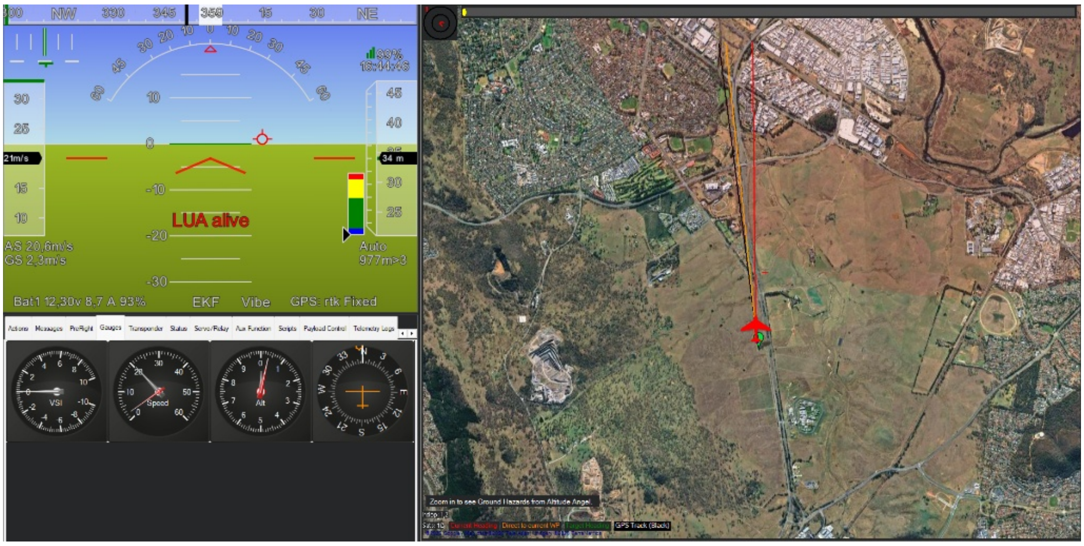

Figure 1.7: Real-time flight path planning and telemetry tracking interface within the Mission Planner ground control station, reflecting modern ArduPilot dynamic waypoint capabilities (Interface source: ArduPilot Mission Planner open-source software).

To look at a more recent article where ArduPilot is used the paper "*An open source synchronized UAV network simulator based on ns-3 and ArduPilot*" by Baidya (2018) [2] discusses how to utilize ArduPilot's UAV simulation engine along with FlyNetSim which is an open source synchronized UAV network simulator which is based on the NS-3 network simulator and the ArduPilot software. One of the most important arguments provided by the authors for the use of ArduPilot is its reputation as a popular software- and hardware-in-the-loop simulator for UAV systems.

1.2.6 Research gap

The topic of UAVs has been greatly studied but there is less viable research into path planning algorithms for UAV. The same goes for "slim" flight paths for conventional fixed-wing aircraft. Prior research emphasizes circular or figure-of-eight orbits for surveillance over wide areas; however, there have been few attempts to construct a theoretical framework to optimize surveillance efficiency by minimizing obstructions by the airframe to cameras. Additionally, how to plan a path for hovering above stall speed for maritime search and rescue (SAR) purposes has yet to be addressed.

1.3 Research Purpose and Objectives

The basic aim of this thesis is to investigate and optimize flight path designs for fixed-wing UAV to be used during maritime Search and Rescue operations. This project focuses on understanding the influence of various wind directions and the impact of the inner loop autopilot control system on the maneuverability and tracking capabilities of the UAV. By investigating these variables, this study intends to solve operational issues currently experienced due to the blocking of the camera's line of sight due to high banking turns of the fuselage and the formation of 'blind spots'. In addition, optimizing flight paths with respect to POIs will help mitigate the impact of environmental issues like sun reflections on water.
This research is intended to serve as the fundamental base that would enable the SSRS to conduct their own autonomous flights in the future, using the proposed pattern to obtain great visibility in high wind. The accumulation of knowledge regarding the impact that the above-listed factors would have on the outcomes of visual observation leads to the identification of the procedure required for achieving the set goals.

1.4 Limitations / Demarcations

There have been several limitations posed in order to keep the research on the topic feasible and focused enough. First and foremost, all the tests involved the use of the ArduPilot Software-in-the-Loop (SITL), which is powerful enough but still lacks the possibility to manage certain characteristics such as specific airframes' measurements, designs and weather carateristics more then wind. As a result, all the findings obtained through this study were achieved within the context of the standard fixed-wing flight mode used in the ArduPlane program.

Secondly, even though SSRS employs mainly "Guided Mode" for real-time adjustment of way points (WP), "Auto Mode" is employed within the course of this study. The rationale for this decision lies in the necessity to create the most symmetrical patterns as well as fully control the geometrical sizes of the figures in question. Thirdly, while the idea of implementing real-time pattern generation through the use of Lua scripting language had been considered, it has not been carried out within the scope of the research due to its limited timeline.

1.5 Thesis outline

The format of this report is designed to take the reader through an understanding of the theoretical basis of the report before moving on to its practical conclusions.

After the introductory chapter, Chapter 2 will go through the theoretical concepts and scientific principles on which the study findings are based as well as the method and reasoning behind choices made along way are described with the SITL simulation environment and the test cycles undertaken for different flight profiles. Chapter 4 presents the empirical evidence, comparing the camera coverage percentage of the existing circular loiter orbits with the innovative "slim" orbits proposed in this paper. And finally chapter 5 goes over and discusses the results and sums up the finds and present a better solution that SSRS can use for certain SAR missions.

2

Methods and Theory

This chapter establishes the combined theoretical framework and experimental methodology utilized to evaluate fixed-wing trajectory performance. It outlines the governing aerodynamic equations and coordinate projection models, describes the technical software ecosystem deployed for high-fidelity simulation, and details the systematic parameter variations used to capture and analyze sensor occlusion data. By pairing mathematical flight physics with an exact Software-in-the-Loop (SITL) testing environment, this approach ensures a repeatable, structurally rigorous platform for evaluating autonomous flight path optimization.

2.1 Research Design and Strategy

In alignment with the operational requirements of the Swedish Sea Rescue Society (SSRS), the core problem statement of this study is organized into four distinct focus areas: pattern geometry, environmental effects, spatial scaling, and coverage optimization.

The proposed research employs a quantitative methodology driven by high-fidelity computer simulations. The structural execution follows an Iterative Development Life Cycle (IDLC) model, wherein initial trajectory modeling is subjected to progressive stress testing. This framework is necessitated by the aerodynamic constraints of the “pseudo-hover” flight envelope, where a conventional fixed-wing aircraft cannot execute zero-airspeed hover maneuvers. Rather than aiming for absolute zero groundspeed, the research design prioritizes flight path optimizations that minimize the tracking radius and maximize sensor dwell time within a localized spatial footprint.

2.2 Theoretical Framework

This section outlines the mathematical and physics-based principles utilized to evaluate fixed-wing trajectory performance. Establishing these concepts is essential for structuring the analytical models, waypoint filters, and subsequent simulation metrics utilized within the methodology.

2.2.1 Aerodynamics of the Pseudo-Hover and Wind Vectors

Unlike multi-rotor platforms, a conventional fixed-wing UAV is a non-holonomic system incapable of zero-airspeed hovering due to its structural dependence on forward velocity to generate aerodynamic lift over its lifting surfaces. To maintain flight, the aircraft's airspeed (V_{air}) must consistently exceed its critical stall speed (V_{stall}). To execute a change in heading, the aircraft must bank at an angle (ϕ), which tilts the lift vector inward to generate the required centripetal force (F_c). In a coordinated level turn, the resulting trajectory radius (R) is governed by the groundspeed (V_{ground}), gravitational acceleration (g), and the bank angle (ϕ):

$$R = \frac{V_{ground}^2}{g \tan \phi} \tag{2.1}$$

As dictated by Equation 2.1, maintaining a tight tracking loop around a localized Point of Interest (POI) requires either a reduction in groundspeed or an increase in the bank angle. However, operating at ultra-low airspeeds or excessive banking attitudes elevates the aircraft load factor, which compromises maneuverability and brings the airframe closer to its aerodynamic stall margin.

This aerodynamic constraint becomes highly complex when operating within a dynamic maritime environment. While aerodynamic lift depends strictly on airspeed (velocity relative to the surrounding air mass), the actual trajectory mapped over the terrain is dictated by the groundspeed vector ($\mathbf{V}_{ground}$), which is the vector sum of the airspeed ($\mathbf{V}_{air}$) and wind velocity ($\mathbf{V}_{wind}$):

$$\mathbf{V}_{ground} = \mathbf{V}_{air} + \mathbf{V}_{wind} \tag{2.2}$$

High operational wind velocities require continuous, high-frequency corrections to both the aircraft heading and bank angle to mitigate drifting. This coupling introduces a spatial mismatch between the local air mass and the target ground track, which directly alters the tracking geometry and sensor visibility profiles.

2.2.2 Spatial Coordinates, Projections, and LOS Geometry

To track and evaluate these trajectories precisely, geodetic coordinates (latitude and longitude) must be mapped into a localized Cartesian frame (x, y, z). Because tactical search and rescue (SAR) operations within the Swedish archipelago typically occur on a localized scale spanning only a few hundred meters, a Local Equirectangular projection is applied. This mathematical approach minimizes computational overhead while maintaining sufficient structural accuracy for waypoint filtering and path visualization:

$$x = (\lambda - \lambda_0) \cdot \cos(\varphi) \cdot 111.320 \tag{2.3}$$

$$y = (\varphi - \varphi_0) \cdot 111.320 \tag{2.4}$$

where φ and λ represent the instantaneous latitude and longitude, φ_0 and λ_0 define the local datum origin, and the constant 111.320 m/deg corresponds to the terrestrial distance of one degree of latitude.

For the pseudo-hover tracking strategy to remain viable, the spatial relationship between the moving aircraft and the stationary POI must be modeled continuously. The relative Line-of-Sight (LOS) vector ($\mathbf{r}_{LOS}$) originating from the aircraft's on-board sensor center to the POI coordinates is expressed in the localized Cartesian frame as:

$$\mathbf{r}_{LOS} = \begin{bmatrix} \Delta E \\ \Delta N \\ \Delta D \end{bmatrix} \tag{2.5}$$

where $\Delta E, \Delta N, \Delta D$ represent the eastward, northward, and vertical down displacements, respectively. To map sensor visibility, this relative translation vector is transformed into body-centric heading (α_h) and elevation (α_v) angles relative to the observer's attitude:

$$\alpha_h = \text{atan2}(\Delta E, \Delta N) - \psi_{yaw} \tag{2.6}$$

$$\alpha_v = \text{atan2}\left(\Delta D, \sqrt{\Delta E^2 + \Delta N^2}\right) \tag{2.7}$$

where ψ_{yaw} represents the instantaneous heading angle of the UAV.

2.2.3 Aerial Occlusion and Sensor Field-of-View Modeling

The payload sensor is evaluated using a geometric angle-of-view enclosure rather than a complex photogrammetric lens distortion profile. This methodology isolates the effects of flight path geometry on target visibility independent of specific optical distortions. A target POI is defined as geometrically contained within the sensor's unoccluded Field of View (FOV) when it satisfies the following angular boundary constraints:

- **Horizontal Boundary:** $|\alpha_h| \leq 135°$
- **Vertical Boundary:** $-90° \leq \alpha_v \leq 0°$

Physical occlusion occurs when the structural airframe—such as the fuselage or wing surfaces—intercepts the sensor's path to the target due to steep rolling maneuvers. To isolate the primary failure modes of specific loitering paths, a hard operational bank threshold of $|\phi| \geq 40°$ is established as the engineering limit for structural blockage. The conditional tracking states are mathematically modeled as:

- If $\alpha_h > 0$ (target situated on the right hemisphere) and $\phi \geq 40°$, the line of sight is structurally occluded.
- If $\alpha_h < 0$ (target situated on the left hemisphere) and $\phi \leq -40°$, the line of sight is structurally occluded.

While a complete optical model would account for precise camera mounting offsets and the aerodynamic dihedral angle of the wings, this discrete threshold provides an accurate, mathematically bounded metric to compare the tracking efficiency of different flight patterns under severe wind constraints.

2.3 Simulation environment and experimental parameters

To eliminate the operational risks of structural airframe damage and vehicle loss associated with deploying unverified flight control algorithms in the field, all testing within this study was executed using a high-fidelity simulation environment. Specifically, the research leverages ArduPilot's Software-in-the-Loop (SITL) simulation engine. The SITL framework executes the exact inner-loop flight control algorithms, navigational state machines, and fail-safe logic deployed on physical autonomous aircraft hardware. Utilizing this simulation engine allows the vehicle's flight dynamics, aerodynamic responses to atmospheric wind forces, and bank-angle attitude limits to be modeled with a high degree of deterministic accuracy.

To ensure software stability and optimal compilation performance, all SITL simulation instances are executed within a Linux environment hosted via Windows Subsystem for Linux (WSL). Autonomous mission profiles, telemetry streaming, and real-time flight tracking are commanded and recorded through the open-source Mission Planner Ground Control Station (GCS) software interface.

To systematically evaluate the performance boundaries of the fixed-wing platform and generate actionable data to support the autonomous operational framework of the Swedish Sea Rescue Society (SSRS), specific environmental conditions and autopilot parameters are varied across testing blocks:

- **SIM_WIND_SPD:** Governs the baseline atmospheric wind velocity, evaluated at discrete increments of 4 m/s, 6 m/s, 8 m/s, and 10 m/s.
- **SIM_WIND_DIR:** Establishes the static horizontal wind vector direction, fixed at 180° to command a continuous atmospheric flow from south to north across the local coordinate system.
- **ROLL_LIM_DEG:** Modulates the maximum allowable airframe bank angle parameter within the autopilot's attitude control loop, constraining the roll limit to isolate the exact onset thresholds of fuselage-induced sensor occlusion.

2.4 Data Collection Tools and Instruments

The instrumentation employed during this experiment was entirely digital, enabling high-frequency log aggregation of the vehicle's flight telemetry. To establish valid scientific conclusions, all testing protocols were maintained within a strictly controlled ecosystem using standardized configurations. Consistency across experimental runs was enforced via a custom mission pattern generator script. This software asset automatically generates standardized waypoint configuration files, adhering strictly to the structural and formatting conventions utilized by the native Mission Planner ground control application. This automation ensures that each generated flight path conforms to identical geometric constraints, eliminating human error from the path synthesis loop.

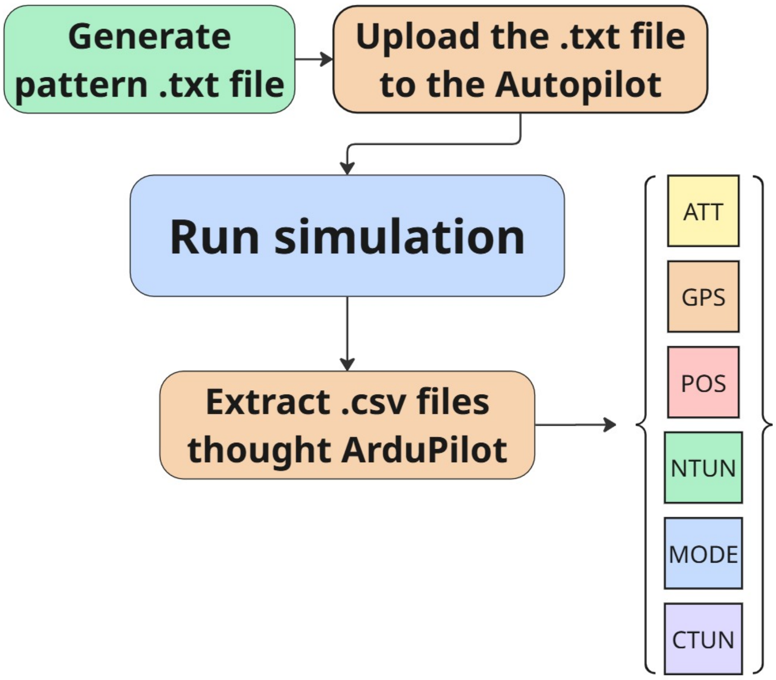

Figure 2.1: Schematic diagram of the data collection and simulation logging procedure.

The path generation scripts grant precise, parametric control over the simulated mission constraints, permitting the modification of loop iteration counts and block scaling factors. Three distinct script classes were engineered to isolate specific experimental variables:

1. **Heading Rotation Script:**
   Progressively rotates the baseline flight trajectory by 5° increments per experimental block to evaluate the impact of varying wind headings on airframe stability and ground-track geometry.
2. **Spatial Scaling Script:**
   Systematically scales down the total boundary dimensions of the flight pattern from 100% to 50% to examine tracking tightness boundaries.
3. **Standard Baseline Orbit Script:**
   Generates the conventional circular loitering flight path currently deployed by the SSRS to establish a control case.

Flight telemetry data is captured using high-resolution MAVLink onboard data flash logs, allowing timestamped state parameters to be sampled down to millisecond intervals. As outlined in the operational flowchart in Figure 2.1, the extracted binary log data is parsed into discrete message channels to extract primary tracking and attitude metrics:

- **ATT:** Records actual versus commanded vehicle attitude (roll, pitch, and yaw angles) to analyze bank angle distribution profiles.
- **GPS:** Captures geodetic coordinates (latitude, longitude, and ellipsoidal altitude), satellite count, and fix status to compile the global ground track.
- **POS:** Logs the fused state estimator positions and velocities to determine instantaneous vehicle velocities (V_{ground}).
- **NTUN:** Tracks target waypoint indexing, cross-track navigation errors, and steering controller response behaviors.
- **CTUN:** Logs inner-loop controller tuning metrics, including commanded throttle settings, achieved airspeeds (V_{air}), and vertical climb rates.
- **MODE:** Provides discrete, timestamped indicators corresponding to the active flight control mode (e.g., *AUTO*, *GUIDED*, *FBWA*, or *RTL*).

2.5 Experimental Procedure

The experimental methodology is structured into three continuous phases to ensure a logical transition from fundamental parameter calibration to formal data logging. This systematic sequence ensures the software constraints of the autopilot framework align directly with maritime aerodynamic conditions.

Phase I: Parameter Calibration and Subsystem Analysis
The initial phase comprised a detailed baseline evaluation of the ArduPilot firmware architecture and its nested PID control loops. Onboard parameters—specifically the maximum bank angle limit and lateral navigation scaling gains—were systematically modulated within exploratory simulation environments. This process isolated the baseline sensitivity profiles of the autopilot, identifying which core navigation parameters dictated trajectory tracking loop stability under tight turning constraints.

Phase II: Trajectory Synthesis and Geometric Modeling
The second phase involved the conceptualization and geometric synthesis of alternative loitering flight paths. Initial path layouts were generated within the Mission Planner graphical user interface to assess basic tracking feasibility across diverse structural forms, including squares, half-circles, zigzag meshes, and dense multi-point arrays. The principal objective was to discover a geometric profile capable of using ambient wind velocity as an aerodynamic braking mechanism, allowing the aircraft to drastically minimize groundspeed over the POI without sacrificing the minimum airspeed required to prevent aerodynamic stall.

Phase III: Execution, Automated Flight, and Telemetry Logging
Following the verification of candidate strategies via manual test flights, the tracking loops were subjected to automated script execution. Automated runs were processed through the SITL simulator across randomized matrix blocks mixing varying wind velocities (`SIM_WIND_SPD`) and autopilot roll constraints (`ROLL_LIM_DEG`). The resulting data streams were parsed from binary storage logs according to the structural schema described in Figure 2.1, establishing a clean dataset for camera coverage and track-error evaluation.

2.6 Data Analysis Techniques

The primary tracking efficiency metric is quantified as a mission success percentage, computed as the ratio of unoccluded sensor operation time to total flight duration over a complete trajectory loop. Beyond area coverage metrics, track compactness is evaluated by measuring the maximum spatial deviation of the UAV's nose-tip relative to the target tracking path.

To compare alternative flight profiles directly with the standard reference case, identical statistical bounds are applied to both configurations. Spatial telemetry tracks are projected onto a local 2D Cartesian plane (X, Y) and rendered using the Python Matplotlib library to map tracking errors visually. The relative spatial profiles of the baseline reference case and the optimized configuration are plotted and verified as illustrated in Figure **??** and Figure **??**, respectively.

2.6.1 Threshold Analysis

Sensor visibility analysis utilizes the 40° critical roll angle threshold established within the theoretical framework. Performance tracking is broken down into two core parameters:

- **Time on Target (ToT):** The cumulative duration during which the UAV remains within the maximum prescribed operational radius from the POI coordinates.
- **Clear View Time:** The cumulative duration during which the sensor's optical field of view remains entirely free from airframe or wing-induced blockage, conditioned on the vehicle's rolling attitude remaining within the unoccluded boundary ($|\phi| < 40^\circ$).

These combined parameters provide the analytic baseline to evaluate the comparative tracking capabilities of the conventional circular loitering circle against the newly proposed high-efficiency trajectories.

2.7 Ethics, Validity, and Reliability

This section addresses the ethical boundaries, experimental reliability controls, and structural validity measures enforced throughout this investigation.

Ethics

There are no adverse ethical implications associated with this study. The research methodology relies exclusively on peer-reviewed academic literature and digital simulations conducted within an open-source software ecosystem. The ArduPilot software core and its corresponding ground control interfaces are distributed under the GNU General Public License v3 (GPLv3). Furthermore, this study involved no human subjects, animal models, or proprietary datasets, and required no structural modifications to the open-source firmware source code.

Reliability

The reliability of the experimental findings is maintained via complete automation of the data generation and recording processes. By utilizing deterministic path-generation scripts paired with a static, containerized SITL environment, all experimental procedures are fully reproducible. Re-execution of the simulation blocks using identical firmware compilations and waypoint parameters will yield identical telemetry datasets.

Validity

Internal validity was established by strictly isolating independent variables across testing blocks; when evaluating the direct impacts of variable roll limits on sensor visibility, inner-loop PID gains and airframe physical limits were held constant. External validity is substantiated by the widespread commercial and industrial deployment of the ArduPilot ecosystem, which forms the operational backbone of professional maritime search and rescue and defense operations globally. Consequently, the dynamic behaviors captured within this simulation framework map directly onto real-world fixed-wing performance characteristics.

2.8 Trajectory development and flight pattern optimization

The development of the optimized loitering trajectory was achieved by balancing the physical constraints of fixed-wing aerodynamics with the operational requirements of localized target tracking. To safely maintain lift and prevent aerodynamic stall, the aircraft was commanded to maintain a minimum airspeed (V_{air}) of 12 m/s relative to the air mass. By strategically utilizing a localized headwind vector as an aerodynamic brake, the flight path was oriented to point directly into an 8 m/s wind current as it approached the Point of Interest (POI). This alignment systematically reduced the aircraft's groundspeed (V_{ground}) to a modest 4 m/s over the target area, maximizing sensor dwell time while maintaining a safe aerodynamic stall margin.

2.8.1 Evaluated and discarded geometries

During the iterative prototyping phase, several alternative flight geometries were rigorously evaluated and subsequently discarded due to structural, logical, or control performance deficiencies:

Crabbing Forward and Half-Circle Geometries: While these patterns successfully maintained continuous target tracking over short intervals, they introduced severe control loops that were highly time-consuming to execute. Additionally, the rapid transitions made it difficult for the inner-loop autopilot to smoothly return the aircraft to its baseline flight path.

Two-Point Loiter Shuttle Pattern: Designed conceptually as a tight linear shuttle pattern between two discrete coordinates, this geometry failed due to the underlying navigational logic of the ArduPilot firmware. The waypoint acceptance radius and trajectory-smoothing algorithms automatically rounded off the sharp corner transitions, turning the path into a standard circular orbit that offered no optical tracking benefits over conventional loitering profiles.

The Square Pattern: This geometry was developed to maximize straight-line tracking segments parallel to the target. However, in high crosswind scenarios, the autopilot was forced to command aggressive crab angles and severe, continuous banking attitudes simply to counteract wind drift and maintain the ground track. This constant rolling attitude resulted in chronic, repetitive fuselage-induced camera occlusion.

2.8.2 Final Trajectory Optimization

The finalized trajectory profile minimizes structural airframe obstructions while preserving robust inner-loop control stability. By scaling up the linear distance between the primary baseline waypoints and introducing a strategic intermediary control point, the updated flight path geometry facilitates sharp, coordinated direction changes at minimal groundspeeds. This optimization increases the percentage of the flight loop dedicated to unoccluded tracking segments, enabling the fixed-wing platform to maintain a continuous, stable line of sight on the maritime POI while actively crabbing to reject dynamic wind drift.

3

Results

This chapter displays the results of data analysis and will be considered in terms of the previously mentioned research objectives. The empirical results will be illustrated using a variety of unprocessed tracking data, processed information on aircraft performance and graphical comparisons between various flight situations.

3.1 Overview of the Evaluation

Analysis has been done on the flights' paths through comparing the initial circular loiter path to the newly generated figure-eight path. This new path design was supposed to generate an area where hovering will take place with minimum lateral translation and repetitive maneuvers. This analysis was performed using software simulation under different waypoints, maximum bank angles, and wind speeds at a constant heading.

In order to properly organize the results obtained, the analysis is split into two main sections: visual results analysis and statistical data analysis.

3.1.1 Visualization

The visual inspection of the trajectory provides the possibility of a direct mapping of the flight limits in physics as well as the behavior of the autopilot system. The visual information provided below can be divided into three types:

Path plots

This graph depicts the (X, Y) ground track of the flight path of the UAV to analyze its accuracy regarding adherence to the set waypoints under varying wind conditions.

Roll-angle during flight

This graph shows the evolution of the aircraft's bank angles over the entire pattern block and helps determine how frequently and how intensely sharp changes in the bank angle occurred.

Coverage during time

Time-series visualization using the binary visibility criterion, showing whether the view from the camera to the target was interrupted at any point in time. The cameras coverage is displayed in figure 3.5.

3.1.2 Data evaluation

In addition to the graphic visualizations, the statistical analysis determines the total efficiency of each individual pattern. The current data set concentrates on two main indicators that affect operations, where the first is coverage percentage. This ratio is calculated through a calculation between the total time of unimpeded visibility and the total time taken by the whole flight operation. The second is the optimized POI location, there the analysis is done to see how changing the POI's location affects the camera's view window.

3.2 Reference Case SSRS: Loiter around POI

The initial path plot is used as the reference maneuver to be compared against the new figure-of-eight maneuver design. The paths formed using the circular pattern generally involve one-sided turns per half cycle, leading to a continuous looping maneuver. Although the use of this circular pattern results in a more natural and smooth trajectory for the pilot to fly, the pattern becomes too big both in terms of space and projected area. This is due to the necessity of maintaining the appropriate airspeed for flying the maneuver to avoid stalling. As an aside, note that the reference data used was captured at an airspeed of 12 m/s, this is not a specifically minimum airspeed used by the SSRS, in order to reduce the number of variables being changed between the reference and optimized test flights. In actual operation, however, the speed is usually set to the standard transit cruise speed of 20 m/s or 15 m/s which SSRS use.

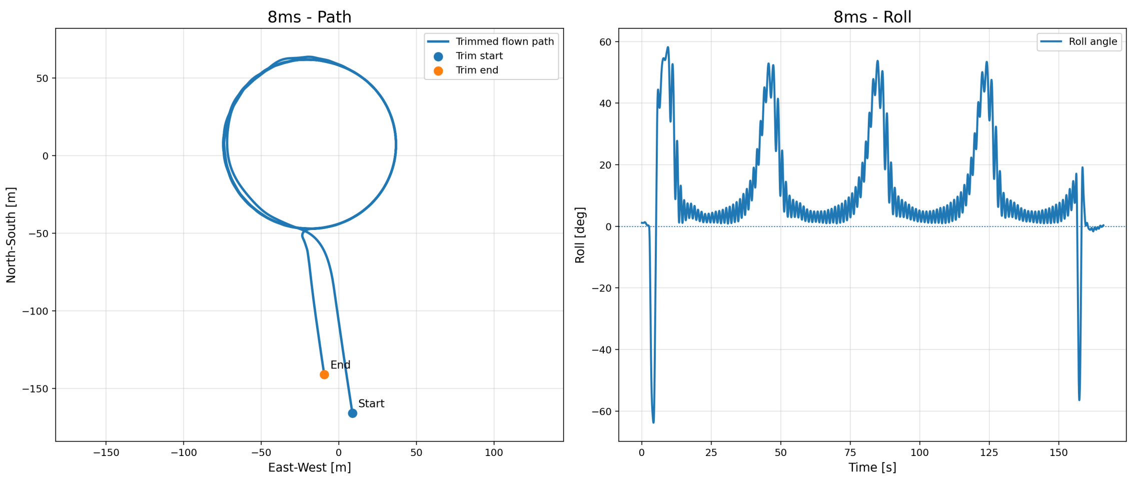

Figure 3.1: Reference loiter pattern along with roll angle graph, wind speed of 8 m/s

In order to prove the validity of the operational problem identified above, the collected data was examined for two types of loiter radius (15 m and 30 m) in terms of how the banking angle varies throughout the flight. When considering the tracking plot under calm conditions, it is obvious that the UAV will have no problems with adhering to the designated trajectory. The problem becomes evident in the examination of the roll angle graph where it is shown that high bank angle spikes become larger, creating substantial coverage issues when there is high wind speed in operation. A clear difference between the roll telemetry at 4 m/s of wind speed and severe 10 m/s conditions is evident. In the course of considering the evaluation of the POI visibility from the camera according to the limits identified theoretically, it is evident that the problem identified initially is correct. It can be clearly stated that there is a decreasing tendency for each stepwise increase in wind speed.

Table 3.1: Blocked percentage depending on wind speed and circle radius for reference case

Circle Radius (m)	Wind Speed (m/s)	Blocked Percentage (%)
30	4	27.46
30	6	26.43
30	8	25.57
30	10	29.33
50	4	10.44
50	6	13.54
50	8	15.70
50	10	23.11

3.3 Proposed Figure-Eight Pattern: General Behavior

This kind of use of the figure-eight design is aimed at reducing the amount of space covered by the movement as well as ensuring that there is a switch from right to left turns periodically. Such an approach leads to oscillations of the roll angle between positive and negative values. The basic advantage of using the figure-eight pattern in this case was to ensure hovering rather than a typical flying path during which there would always be forward motion. As mentioned above, in the methodology section, a further analysis of this specific pattern was undertaken using simulations. Through tests and tweaking the autopilot parameters, it became possible to define the range of the bank angle required for optimal tracking control as well as identifying the minimal amount of banking necessary to accommodate the design. Wind conditions that give aerodynamic assistance were defined to provide the sharpest turns without having the camera covered for long, as well as establishing the smallest size of the pattern that can be flown without reducing flight performance.

3.3.1 Bankangle limitation

As for the analysis of the banking angle impact and its role in changing the flight dynamics via the telemetry logs, one may observe a definite tendency towards stability with the reduction of the set ROLL_LIM_DEG parameter value in the autopilot. The disadvantage of having a smaller roll angle, however, comes in the necessity for the aircraft to perform a much wider turn to accomplish the required action.Studying the boundaries between 45° and 65° values, which are adjustable in 5° increments, we come to certain conclusions. As running the simulation with smaller roll angle implies less risk of camera coverage loss on ordinary tracking segments due to the minimum allowed angle being 5° above the 40° camera blockage level, the additional need for the wider turn increases the portion of flight when the plane needs to fly straight ahead with maximum allowed bank. The percentages of flights accomplished according to the described pattern and with various wind speed levels are shown in the table below.

Table 3.2: Percentage of proposed pattern spent at maximum allowed roll limit.

Roll Limit	**4 m/s**	**6 m/s**	**8 m/s**	**10 m/s**
RL45	37.69	17.84	6.63	5.02
RL50	27.18	8.93	5.61	3.45
RL55	9.45	3.37	2.80	1.37
RL60	0.98	0.86	0.88	1.03
RL65	0.91	0.94	1.01	0.88

Based on these individual variations in performance levels, it can be determined that between flight stability and tracking performance, it is optimal to have the ROLL_LIM_DEG set to 60°. It is not a case that having a limit set to 65° makes the system much more inferior since the raw coverage data shows almost no difference and the 60° provide a bit more stable maneuverability. The reason why a lower limit for the maximum roll is beneficial is due to the reduction in the severity of the degree-shift range, which needs to be done during rolling to the right side. The only advantage that comes with setting the bank angle to 65° is the possibility of taking tighter turns, resulting in more compact spatial patterns, which will be reviewed later in section 4.3.3 Pattern size.

3.3.2 Wind direction

In order to determine the required precision of the pattern positioning relative to the real-time conditions, relative wind direction testing has been carried out. How does the UAV perform the exact same pattern after being influenced by wind directed differently? This particular question had been analyzed while moving around the 360° circle. As the geometry of the chosen pattern is designed to make use of wind direction as an aerodynamic brake, the rotation of a pattern by 180° relative to wind direction leads to the complete destruction of flight logic and tracking performance.

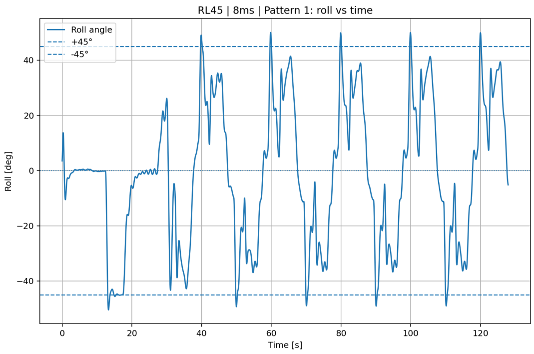

(a) Roll limit set to 45 degrees, wind speed set to 8 m/s

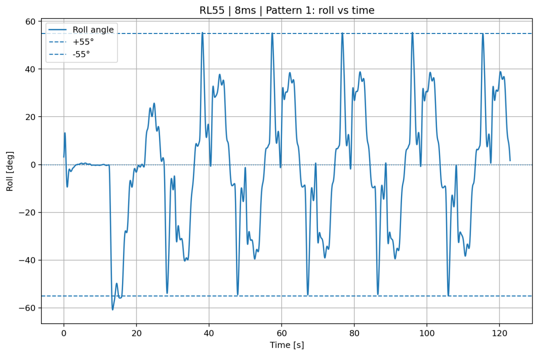

(b) Roll limit set to 55 degrees, wind speed set to 8 m/s

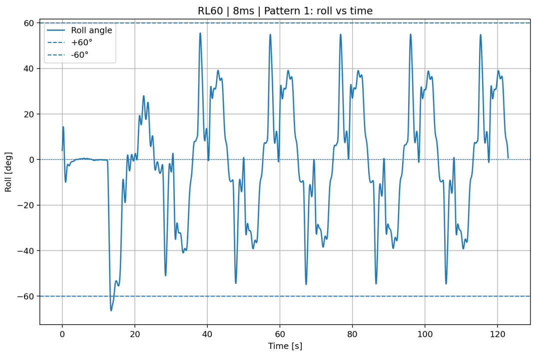

(c) Roll limit set to 60 degrees, wind speed set to 8 m/s

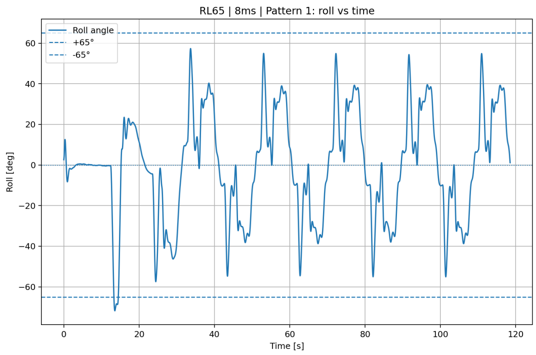

(d) Roll limit set to 65 degrees, wind speed set to 8 m/s

Figure 3.2: Banking change during flight with different RDL set with a wind speed at 8ms

To establish operational tolerance, the wind was aligned with the baseline and the pattern tested while being rotated with the help of 5° steps. It was proved that according to active wind speeds, the maximum possible tolerance to wind directions is ±35°. What's more, wind speeds higher than average provided a clearer pattern completion in terms of this tolerance. Thus, it should be said that using such a pattern in the real world, one doesn't need to align it precisely with the direction of the wind.

3.3.3 Pattern Size

As indicated throughout this experiment, reducing the physical dimensions of the pattern makes the fixed-wing aircraft design approach hover capabilities similar to those of the quadcopter. From the initial pattern design that is not scaled down, it will take a minimum of 120 seconds for the flight to cover four repetitions of the designed pattern. This is dependent on the wind velocity and the maximum roll allowed. In order to obtain the pattern of the smallest dimension but with accurate tracking capabilities, the pattern was resized gradually. For original size and measurements see figure 3.3.

With the help of the script that was designed to guarantee mathematical accuracy and reliability of the data provided, the pattern was reduced from 100% down to 50% in regular 10% increments. Such scaling enabled precise verification regarding the spatial scale at which the pattern would be compact enough to perform further analysis in terms of camera coverage. As it can be seen in the visualization of the telemetry data, the reduction at 50% of scale was not capable of ensuring the turn entry criteria. Hence, there were oversights. In contrast, the pattern scaled down to 60% proved to be sufficiently compact and was able to keep within the desired bounds. Therefore, the minimal geometric scale at which the suggested pattern may be implemented is 60%. This scaling will make sure to compress the flight time of the block into around 100 seconds. Furthermore, the restrictions regarding the roll angle of 45° and 50° were omitted in the current set of tests, since they were previously found to be lacking turning capabilities.

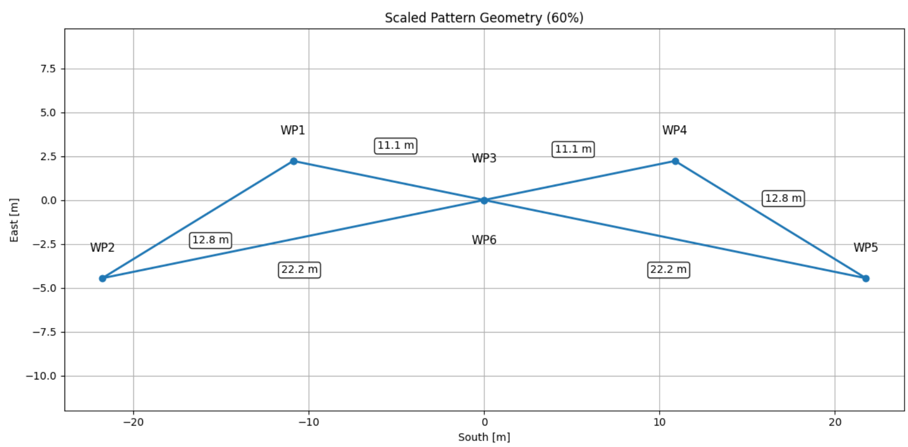

Figure 3.3: Proposed pattern 60% size

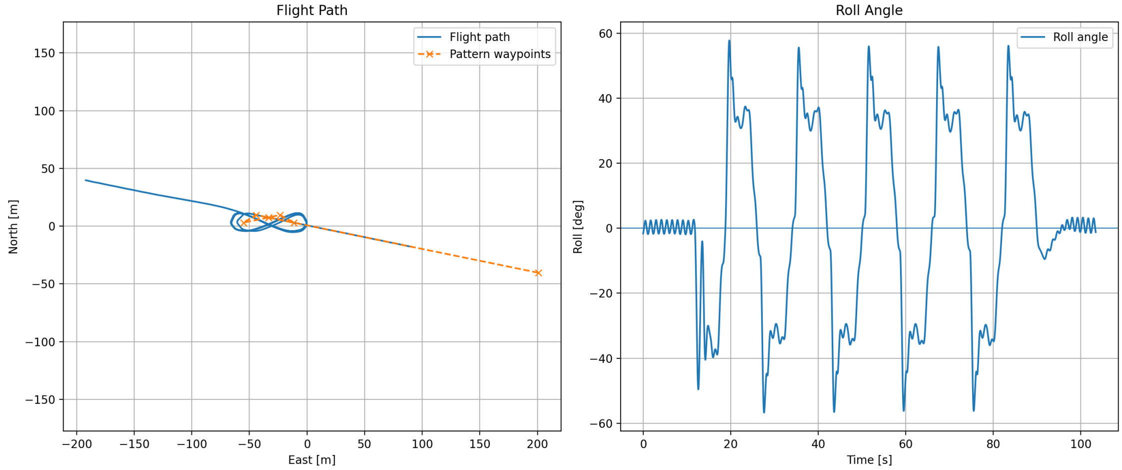

Figure 3.4: Proposed pattern at 60% size along with bank angle graph

3.4 Camera coverage

This is one of the key points of evaluating the efficiency of this solution, as its effectiveness can be determined by its practical applicability and superiority compared to the baseline. Stable trajectories, ability to operate under different wind velocities and different roll angles as well as tolerance of slight wind misalignment are relevant only if there is no obstruction in the line of sight of the camera. With the help of defining criteria when the camera was obstructed by objects and testing this parameter against all sets of collected data, the efficiency of this proposed solution will be evaluated compared to the currently used active solution of SSRS.

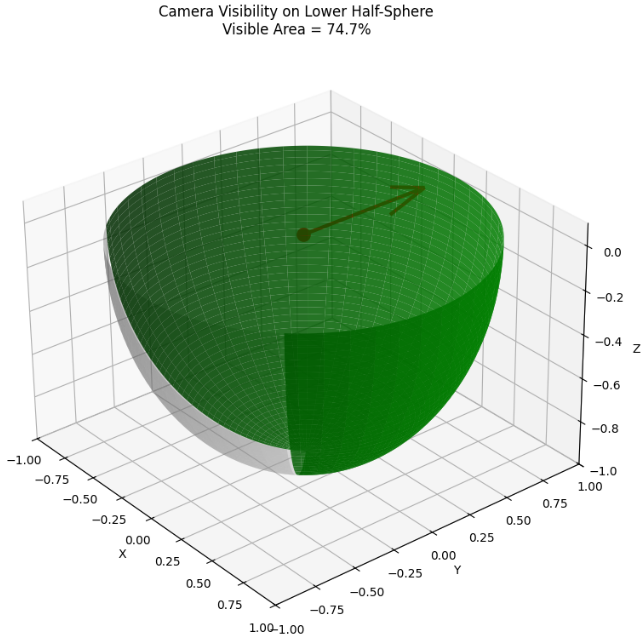

Figure 3.5: The cameras FOV

The rules for evaluation are stated as described in Chapter 2.4. The simulation of the camera's sensor assumes a horizontal movement within the range of $-135° - +135°$ as well as vertical movement within the range of $0°$ to $-90°$. The figure 3.5 displays the field of vision of the camera. It is important to understand that this model assumes analysis of the lens direction of the camera as a directional vector and not a volume; the volume would depend heavily on the actual distance to the object.

With these angles taken into account, the camera is theoretically able to cover 74.7% of its surroundings around the underside of the drone under no interference from the airframe. The POI for the reference case simulation scenarios was placed right at the center of the loitering circle, at an altitude of 30 m. In the new proposed pattern simulation scenarios, the POI was set 30 m south from the intersection way point of the two lines, again at an equal altitude of 30 m.

The strict occlusion criterion implies that any bank angle of 40° or greater from the closest wing to the POI leads to an overall occlusion result. In practical applications, the actual point where partial or total occlusion occurs will be based on the specific position of the camera. Analyzing all of the data with the occlusion engine results in the following matrices:

Table 3.3: Blocked percentage for proposed pattern depending on roll limit and wind speed

Roll Limit	**4 m/s**	**6 m/s**	**8 m/s**	**10 m/s**
RL45	44.14	32.81	11.30	7.45
RL50	38.67	30.48	10.00	6.82
RL55	36.92	29.58	9.29	7.65
RL60	36.58	29.54	8.78	7.04
RL65	35.99	28.18	8.91	6.24

Table 3.4: Blocked percentage for RL55 depending on wind direction angle and wind speed

Wind Approch Angle (°)	**4 m/s**	**6 m/s**	**8 m/s**	**10 m/s**
5	36.92	29.58	9.29	7.65
10	34.18	26.13	7.80	4.60
15	40.80	23.20	10.29	4.89
20	43.58	28.68	13.93	5.22
25	44.50	31.62	17.70	8.14
30	46.32	33.14	18.81	10.13
35	56.75	44.26	27.96	12.20

Table 3.5: Blocked percentage for RL65 depending on pattern scale and wind speed

Pattern Scale (%)	**4 m/s**	**6 m/s**	**8 m/s**	**10 m/s**
90	49.19	36.79	7.93	5.26
80	51.93	40.18	8.12	6.05
70	61.11	49.08	8.75	5.11
60	60.79	54.26	12.59	6.49

Considering the total gathered data, it becomes evident that even if you scale down the pattern 60% of its original size, see figure 3.3, the coverage is still better then the reference case for both **8 m/s** and **10 m/s**.

3.4.1 Coverage for different POI location

Spatial flexibility with regard to the POI positioning is another critical operational consideration. To ensure that the end result is a reproduction of the maneuverability exhibited by a quadcopter, the system should be capable of taking pictures from various angles to give different views for the rescuers. In the classic example where the reference was circular, it was possible to have a complete 360° horizontal angle view of the object during rotation since there was no obstruction from the airframe.

To test if the same multi-view can be achieved using the suggested figure-eight approach, systematic movement of the POI was conducted while maintaining constant distance and altitude relative to the reference way point.

- **Altitude** - 30 meter
- **Cirular radius seen from WP3/WP6** - 30 meter
- **Degree increments around circle** - 5 degrees

Using the identical visibility and occlusion rules for the aircraft based on the rearranged POI matrix, one can determine whether a traditional fixed-wing UAV can be used for taking multi-angle pictures in a way similar to that performed by the rotary-wing UAV.

Table 3.6: Top 10 POI placements with the highest visibility percentage.

Rank	RL	Wind [m/s]	Wind Angle [°]	POI [°]	Visible [%]
1	50	10	10	100	96.42
2	55	10	10	205	96.08
3	60	10	10	205	96.06
4	65	10	10	205	95.85
5	45	10	10	205	95.44
6	55	10	10	180	95.40
7	55	10	15	180	95.11
8	55	10	20	180	94.78
9	65	10	0	180	93.76
10	50	10	0	180	93.18

Based on the data in the location matrix, see table 3.6, it is clear that the pattern do have for fairly good ability to taking multi-angle pictures in a way similar to that performed by the rotary-wing UAV. The size is kept at its original size, see figure **??**. Looking at the POI location sweep plot, its clear in which areas its most optimal per wind approach angle, wind speed or roll limit angle, figure 3.6 displays the best POI location along the 30 meter radius circle.

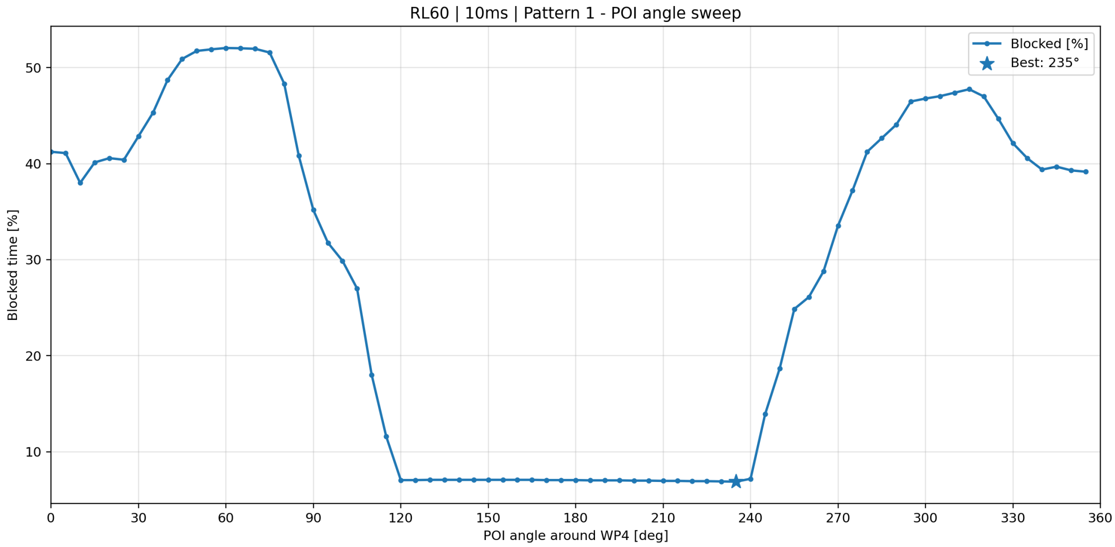

Figure 3.6: POI location sweep for the proposed pattern, 10 m/s

4

Discussion and Conclusion

4.1 Discussion

The objective of this thesis was to investigate whether a conventional fixed-wing UAV could achieve a so called "pseudo-hover" behavior that is suitable for maritime Search and Rescue operations while maintaining acceptable camera visibility and flight stability under varying wind conditions. Through the use of ArduPilot SITL simulations, telemetry analysis, and custom-generated flight patterns, it has been shown that the proposed figure-eight pattern, see figure **??**, provides several operational advantages compared to the currently used circular loitering approach, see figure 3.1.

Looking at the results, they demonstrate that the standard circular loiter pattern becomes increasingly more problematic for each increased wind step due to the required steep bank angles that is needed to maintain the orbit around the point of interest. This directly correlates to the increase in the amount of time during flight in which the aircraft's own body obstructs the camera view. The collected reference data showed that the circular pattern produced blockage percentages that exceeded 29% at 10 m/s wind speed for a loiter pattern with $30m$ radius. Even with a larger radius of $50m$, the blockage did increase significantly as wind speed increased. This directly relates to the problem description and points to possible improvements.

The figure-eight pattern or also called proposed new pattern, see figure **??**, do address this issue by alternating the turning direction and introducing longer straight tracking segments with less active banking. This did result in a reduced duration of continuous banking. Which did then lead to improved visibility toward the POI. The pattern effectively used the wind as an aerodynamic braking mechanism, which did allow the fixed-wing UAV to maintain sufficient airspeed above stall while simultaneously reducing its groundspeed over the target area. This behavior did allow the UAV to effectively use certain hovering characteristics normally associated with multi-rotor systems, without limitations of rotary-wing when it comes to weight and energy consumption.

To highlight one of the more important findings during this research do concern the relationship between roll limitation and flight performance. By analyzing the Roll angle graphs during flight time, the conclusion that a lower roll limit did reduced the severity of banking maneuvers but simultaneously increased the required turning radius which did reduce tracking precision for smaller patterns with tighter turns. On the other hand, a higher roll limit did make it possible to scale down the pattern size without interfering too much with the maneuvers but introduced slightly longer temporary camera blockage. The analysis showed that a roll limit between 55° and 65° provided the best overall compromise between maneuverability, pattern compactness, and camera visibility. In particular, RL60 produced nearly identical blockage performance to RL65 while maintaining smoother and more stable flight behavior, and also a bit better then the RL55.

When looking at the Swedish archipelago and other coastal locations where the SSRS drones will in the future be available to assist in active SAR missions. These areas are mostly open and due to that the wind becomes a big factor, according to SMHI, “Swedish Meteorological and Hydrological Institute” the average wind speed in Gothenburg’s archipelago is between $6 - 8$ m/s. So the influence of wind speed and direction is also significant to verify that the pattern does function in real life weather conditions. Since the proposed flight logic intentionally uses the wind as part of the maneuvering strategy, the orientation of the pattern relative to the wind vector became important. Through the simulation it is shown that the pattern maintained acceptable functionality within approximately ±35° relative wind misalignment. Beyond this range, tracking quality deteriorated quickly and the aerodynamic braking effect was reduced since it also works as an accelerating force. However, the relatively large tolerance range indicates that the pattern could still be practical in real maritime operations where wind conditions continuously change.

Investigations into the pattern scalability did demonstrate that it is also an important limitation of fixed-wing pseudo-hover operation. Reducing the size of the pattern improved localization around the POI and shortened the total mission duration, but just barely, but excessive down scaling the pattern size did reduced the aircraft’s ability to complete the turns correctly. Simulations did result in that a scaling factor down to 60% represented the smallest reliable configuration before tracking overshoots and maneuvering instability became excessive. Even at this reduced size, the proposed pattern still achieved better visibility performance than the reference loiter pattern, not depending on loiter radius, under higher wind conditions.

The camera coverage analysis did confirm that the proposed pattern did substantially improve operational effectiveness during stronger winds. While the figure-eight pattern performed worse than the circular loiter during low wind conditions. As shown in table 4.1 the optimized pattern became increasingly advantageous as wind speed increased.

Table 4.1: Best pattern for the different wind speeds.

Wind speed [m/s]	**Pattern name**	**Visibility percentage**	POI location
4	Loiter R50	89.56	Center
6	Loiter R50	86.46	Center
8	Figure of 8 RL65	91.09	180
10	Figure of 8 RL50	96.42	100

This is particularly relevant for maritime SAR operations, where environmental conditions can often be unfavorable. At 8 m/s and 10 m/s wind speeds, the proposed pattern consistently reduced blockage compared to the reference case. The results therefore suggest that the pattern is more suitable for surveillance missions in harsh-wind conditions where the conventional loitering begins to fail in visibility.
Next up it is also demonstrated that a fixed-wing UAV can achieve reasonable results for multi-angle observation capability similar to that of rotary-wing by repositioning the POI relative to the pattern geometry. The optimized POI placements did result in a reduced blockage percentages to values even below 5% in some scenarios. This suggests that careful geometric placement of the target area can significantly improve operational image capturing without requiring major modifications to the airframe or reconfiguration of the autopilot system.
Despite the positive findings, there are several limitations still present. Since all testing was conducted within the ArduPilot SITL simulation environment, meaning that environmental factors like turbulence, gusting winds, sensor noise, sea spray, and real aerodynamic disturbances were not fully represented. In addition, the occlusion model used in this thesis was intentionally simplified and based on a fixed roll-angle threshold rather than a detailed optical or geometric camera model. The actual visibility characteristics in real-world applications will depend heavily on camera mounting position, wing geometry, and lens specifications. Furthermore, only one fixed-wing flight platform and one flight logic structure were investigated. The use of UAV configurations and design like the one used by SSRS may produce different aerodynamic responses and tracking characteristics.

4.1.1 Future work

Future work done in this field should therefore focus on validating the proposed flight pattern through real-world flight experiments. Particular emphasis should be placed on testing under dynamic maritime weather conditions and integrating more advanced visibility models that account for sun glare, wave reflections, and true camera projection geometry. Use of an image identification large language model (LLM) like YOLO could be used for calculation of real time POI visibility by helping to identify how many frames that get affected by the fixed-wing UAVs body.

Another interesting continuation would be to implement a real-time path generation using LUA scripting inside ArduPilot. This could allow the user to control the UAV in "GUIDED MODE" and manually place the pattern in relation to the POI. This can also let the user rotate and scale the pattern according to live wind telemetry data. Additional studies could also investigate hybrid VTOL platforms that combine the endurance advantages of fixed-wing aircraft with the hovering capabilities of rotary-wing systems, which SSRS is currently looking into.

4.2 Conclusion

In conclusion, this thesis demonstrates that the presented optimized figure-eight flight patterns would in practice significantly improve the operational camera coverage of fixed-wing UAVs during maritime SAR missions compared to conventional used circular loitering pattern. By combining controlled roll limitations, wind-assisted maneuvering, and optimized POI placement, the proposed "pseudo-hover" concept does enable a fixed-wing UAV to maintain both a stable and compact surveillance behavior while still preserving the advantages associated with aerodynamic flight and low energy consumption. The results provide a technical foundation for possible future development of autonomous flight strategies within the Swedish Sea Rescue Society drone program and do contribute toward broader research into the efficiency of UAV surveillance in challenging environments.

Bibliography

[1] Ajaj, R. M., Friswell, M. I. (2018). Aeroelasticity of compliant span morphing wings. *Smart Materials and Structures, 27*(10), 105052.

[2] Baidya, S., Shaikh, Z., Levorato, M. (2018, October). Flynetsim: An open source synchronized UAV network simulator based on ns-3 and ArduPilot. In *Proceedings of the 21st ACM International Conference on Modeling, Analysis and Simulation of Wireless and Mobile Systems* (pp. 37–45).

[3] Barringer, L. B. (1938). Soaring. *Journal of Air Law and Commerce, 9*, 97–107.

[4] Belardo, M., Paletta, N., Di Palma, L., Pecora, M. (2014). Structural and Aeroelastic Design of a Joined-Wing UAV. *Journal of Aerospace Engineering, 27*(1), 93–111.

[5] Bin, H., Justice, A. (2009). The design of an unmanned aerial vehicle based on the ArduPilot. *Indian Journal of Science and Technology, 2*(4), 12–15.

[6] Boslough, M. (2017). Autonomous dynamic soaring. In *2017 IEEE Aerospace Conference* (pp. 1–20). IEEE.

[7] Jeon, I., Ham, S., Cheon, J., Klimkowska, A. M., Kim, H., Choi, K., Lee, I. (2019). A real-time drone mapping platform for marine surveillance. *The International Archives of the Photogrammetry, Remote Sensing and Spatial Information Sciences, XLII-2/W13*, 385–391.

[8] Kubiak, T., Dudzinski, L., Fellner, R., Feltynowski, M., Czyżewski, Ł. (2025). Use of unmanned aerial vehicles by the entities of National Firefighting and Rescue System in Poland to search for people – a review of interventions performed in the years 2021–2023. *International Journal of Emergency Services, 14*(1), 41–51.

[9] Lattimer, B. Y., Huang, X., Delichatsios, M. A., Levendis, Y. A., Kochersberger, K., Manzello, S., Franks, P., Jones, T., Salvador, J., Delgado, C., Angelats, E., Parès, E., Martín, D., McAllister, S., Suzuki, S. (2023). Use of Unmanned Aerial Systems in Outdoor Firefighting. *Fire Technology, 59*(6), 2961–2988.

[10] Messmer, M., Kiefer, B., Varga, L. A., and Zell, A. (2024). *UAV-assisted maritime search and rescue: A holistic approach.* arXiv preprint arXiv:2403.14281.

[11] Allen, M. J. (2007). *Autonomous Soaring for Unmanned Aerial Vehicles.* NASA Technical Memorandum, Dryden Flight Research Center, TM-2007-214611.

[12] Panagiotou, P., Yakinthos, K. (2020). Aerodynamic efficiency and performance enhancement of fixed-wing UAVs. *Aerospace Science and Technology, 99*, 105575.

[13] Perez-Saura, D., Fernandez-Cortizas, M., Perez-Segui, R., Arias-Perez, P., Campoy, P. (2023). Urban Firefighting Drones: Precise Throwing from UAV. *Journal of Intelligent & Robotic Systems, 108*(4), 66.

[14] Pettersson, E. (2020). *Design of a drone system for maritime search and rescue missions*. Master's Thesis, KTH Royal Institute of Technology.

[15] Pucci, D. (2012). Flight dynamics and control in relation to stall. In *2012 American Control Conference* (pp. 118–124). IEEE.

[16] Ribeiro, P., Coelho, A., Campos, R. (2025). On the energy consumption of rotary-wing and fixed-wing UAVs in flying networks. In *2025 20th Wireless On-Demand Network Systems and Services Conference (WONS)* (pp. 1–4). IEEE.

[17] Reddy, G., Wong-Ng, J., Celani, A., Sejnowski, T. J., Vergassola, M. (2018). Glider soaring via reinforcement learning in the field. *Nature, 562*(7726), 236–240.

[18] Silvagni, M., Tonoli, A., Zenerino, E., Chiaberge, M. (2017). Multipurpose UAV for search and rescue operations in mountain avalanche events. *Geomatics, Natural Hazards and Risk, 8*(1), 18–33.

[19] Sukumar, P. P., Selig, M. S. (2010). Dynamic Soaring of Sailplanes over Open Fields. In *28th AIAA Applied Aerodynamics Conference* (p. 4953). https://doi.org/10.2514/6.2010-4953

[20] Sukumar, P. P., Selig, M. S. (2013). Dynamic soaring of sailplanes over open fields. *Journal of Aircraft, 50*(5), 1420–1430.

[21] Ünlüsoy, L., Yaman, Y. (2017). Aeroelastic behaviour of UAV wings due to morphing. *Aircraft Engineering and Aerospace Technology, 89*(1), 30–38.

[22] Ye, J., Wang, J., Song, T., Wu, Z., Tang, P. (2021). Nonlinear modeling the quadcopter considering the aerodynamic interaction. *IEEE Access, 9*, 134716–134732.

A
Appendix 1

A.1 Patterns, Roll graphs and Coverage plots

A.1.1 Wind approch angle evaluation pattern for RL 60, wind speed 8 m/s

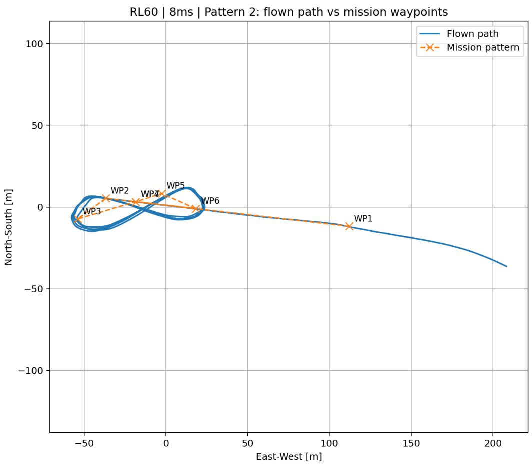

(a) Roll limit set to 65 degrees, wind approch angle set to 5

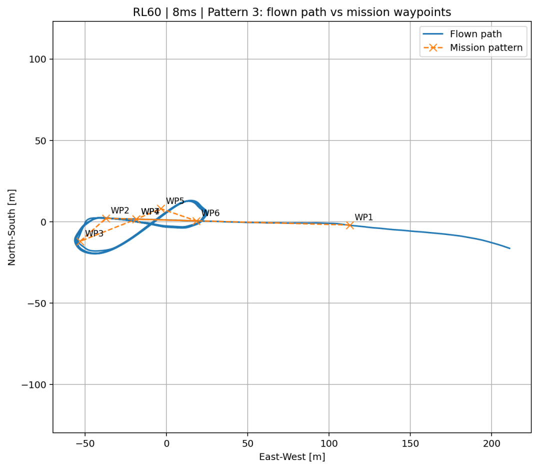

(b) Roll limit set to 65 degrees, wind approch angle set to 10

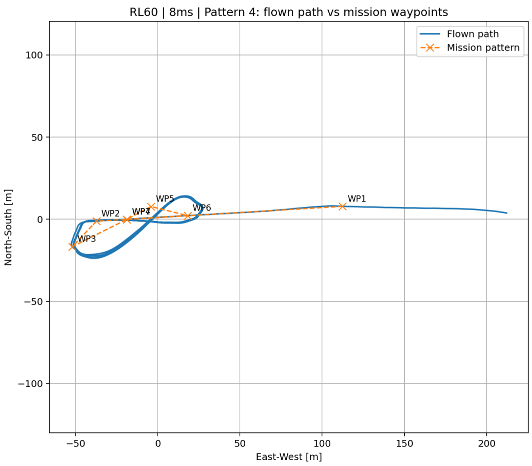

(c) Roll limit set to 65 degrees, wind approch angle set to 20

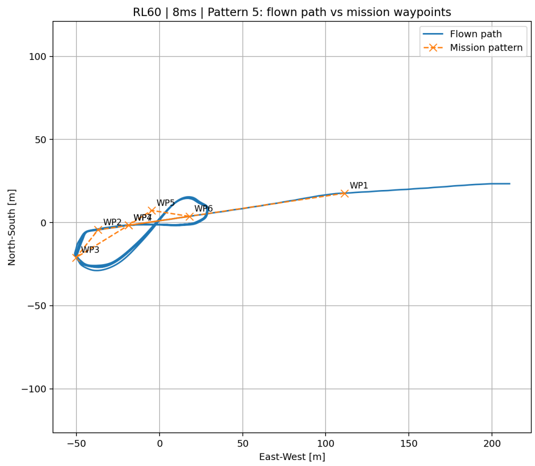

(d) Roll limit set to 65 degrees, wind approach angle set to 25

Figure A.1: Pattern plots for different wind approch angles and set with RDL65 and wind speed at 8ms

A.1.2 Roll angle grapths for RL65, wind speed 8 m/s

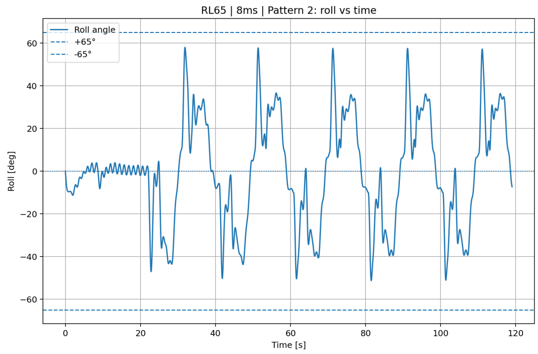

(a) Roll limit set to 65 degrees, wind approch angle set to 5

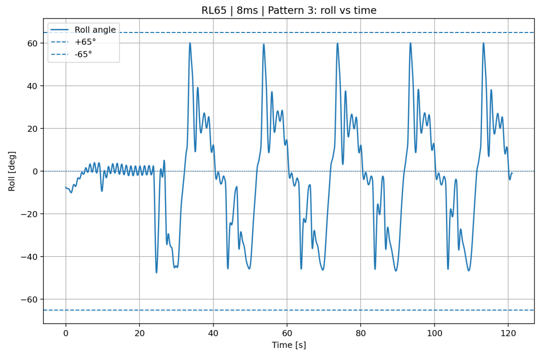

(b) Roll limit set to 65 degrees, wind approch angle set to 10

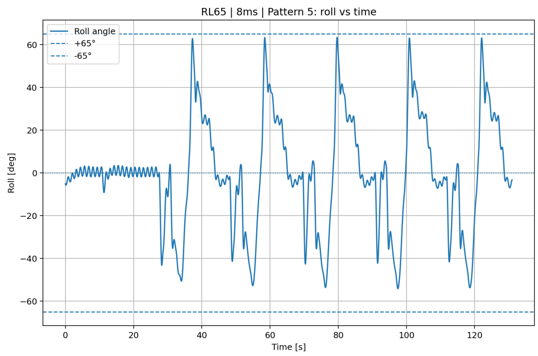

(c) Roll limit set to 65 degrees, wind approch angle set to 15

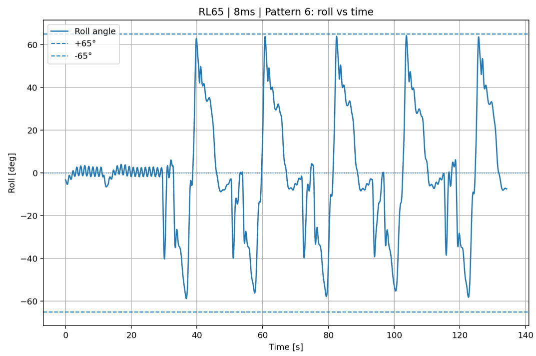

(d) Roll limit set to 65 degrees, wind approach angle set to 2

Figure A.2: Banking change during flight with different wind approch angles and set with RDL65 and wind speed at 8ms

A.2 Flight pattern .txt

A.2.1 Wind direction test

The following listing shows partial section of the QGroundControl waypoint mission used for the figure-eight flight experiments. The mission contains seven repeated flight pattern blocks with incremental rotational offsets and repeated DO_JUMP commands for sustained flight evaluation.

Listing A.1: Partial QGroundControl mission file used for wind direction experiments

```
QGC WPL 110
0   0   0   16  0.000000    0.000000    0.000000    0.000000
        -35.363262  149.165237  584.099976  1
1   0   3   22  15.000000   0.000000    0.000000    0.000000
        0.000000    0.000000    10.000000   1
2   0   3   16  0.000000    0.000000    0.000000    0.000000
        -35.360216  149.164734  75.000000   1
3   0   0   178 0.000000    12.000000   0.000000    0.000000
        -35.360216  149.164734  0.000000    1
4   0   3   16  0.000000    0.000000    0.000000    0.000000
        -35.357171  149.164231  100.000000  1
5   0   3   16  0.000000    0.000000    0.000000    0.000000
        -35.356901  149.162612  100.000000  1
6   0   3   16  0.000000    0.000000    0.000000    0.000000
        -35.357001  149.162412  100.000000  1
7   0   3   16  0.000000    0.000000    0.000000    0.000000
        -35.356934  149.162812  100.000000  1
8   0   3   16  0.000000    0.000000    0.000000    0.000000
        -35.356901  149.162990  100.000000  1
9   0   3   16  0.000000    0.000000    0.000000    0.000000
        -35.357001  149.163212  100.000000  1
10  0   3   16  0.000000    0.000000    0.000000    0.000000
        -35.356934  149.162812  100.000000  1
11  0   0   177 5.000000    4.000000    0.000000    0.000000
        0.000000    0.000000    0.000000    1
12  0   3   16  0.000000    0.000000    0.000000    0.000000
        -35.356754  149.161733  100.000000  1
13  0   3   16  0.000000    0.000000    0.000000    0.000000
        -35.356600  149.160092  100.000000  1
14  0   3   16  0.000000    0.000000    0.000000    0.000000
        -35.356714  149.159903  100.000000  1
15  0   3   16  0.000000    0.000000    0.000000    0.000000
        -35.356619  149.160294  100.000000  1
```

A.2.2 Resizing the proposed pattern for verification

The following listing shows partial section of the QGroundControl waypoint mission used for the figure-eight flight experiments. The mission contains six repeated flight pattern blocks with incremental size changes and repeated `DO_JUMP` commands for sustained flight evaluation.

Listing A.2: Partial QGroundControl mission file used for pattern size experiment

```
QGC WPL 110
0   0   0   16  0.000000    0.000000    0.000000    0.000000
                -35.363262  149.165237  584.099976  1
1   0   3   22  15.000000   0.000000    0.000000    0.000000
                0.000000    0.000000    10.000000   1
2   0   3   16  0.000000    0.000000    0.000000    0.000000
                -35.360216  149.164734  50.000000   1
3   0   0   178 0.000000    12.000000   0.000000    0.000000
                -35.360216  149.164734  0.000000    1
4   0   3   16  0.000000    0.000000    0.000000    0.000000
                -35.357171  149.164231  100.000000  1
5   0   3   16  0.000000    0.000000    0.000000    0.000000
                -35.356721  149.161533  100.000000  1
6   0   3   16  0.000000    0.000000    0.000000    0.000000
                -35.356821  149.161333  100.000000  1
7   0   3   16  0.000000    0.000000    0.000000    0.000000
                -35.356754  149.161733  100.000000  1
8   0   3   16  0.000000    0.000000    0.000000    0.000000
                -35.356721  149.161911  100.000000  1
9   0   3   16  0.000000    0.000000    0.000000    0.000000
                -35.356821  149.162133  100.000000  1
10  0   3   16  0.000000    0.000000    0.000000    0.000000
                -35.356754  149.161733  100.000000  1
11  0   0   177 5.000000    4.000000    0.000000    0.000000
                0.000000    0.000000    0.000000    1
12  0   3   16  0.000000    0.000000    0.000000    0.000000
                -35.356664  149.161193  100.000000  1
13  0   3   16  0.000000    0.000000    0.000000    0.000000
                -35.356214  149.158496  100.000000  1
14  0   3   16  0.000000    0.000000    0.000000    0.000000
                -35.356304  149.158316  100.000000  1
15  0   3   16  0.000000    0.000000    0.000000    0.000000
                -35.356244  149.158675  100.000000  1
16  0   3   16  0.000000    0.000000    0.000000    0.000000
                -35.356214  149.158835  100.000000  1
```

A.2.3 Extracted referent QGroundControll mission

The following listing shows a partial section of the manually created way point mission used as reference when creating the automated mission generator script was created.

Listing A.3: QGroundControl manual reference mission

```
QGC WPL 110
0   0   0   16  0.000000    0.000000    0.000000    0.000000
        -35.363262  149.165237  584.099976  1
1   0   3   22  15.000000   0.000000    0.000000    0.000000
        0.000000    0.000000    10.000000   1
2   0   3   16  0.000000    0.000000    0.000000    0.000000
        -35.357784  149.164445  50.000000   1
3   0   0   178 0.000000    12.000000   0.000000    0.000000
        0.000000    0.000000    0.000000    1
4   0   3   18  4.000000    0.000000    0.000000    0.000000
        -35.355001  149.163952  50.000000   1
```

DEPARTMENT OF MECHANICS AND MARITIME SCIENCES
CHALMERS UNIVERSITY OF TECHNOLOGY
Gothenburg, Sweden 2026
www.chalmers.se

CHALMERS
UNIVERSITY OF TECHNOLOGY